Scanning Transmission Election Microscopy Observations of Twisted Epitaxial Gold Nanodiscs in Twisted Molybdenum Disulfide Bilayers

Yi Cui (崔一)*, Pawel Czaja, Yi Cui (崔屹) and Robert Sinclair*

Department of Materials Science and Engineering, Stanford University; Stanford, 94305, USA.

*Corresponding author. Email: cuiy@stanford.edu, bobsinc@stanford.edu.

Abstract

Atomic scale, scanning transmission electron microscopy (STEM) analysis of the moiré structures in twisted epitaxial gold nanodiscs encapsulated in twisted bilayer molybdenum disulfide is presented. High angle annular dark field STEM imaging reveals that the period of the moiré patterns between gold and molybdenum disulfide varies with different twist angles of the bilayer molybdenum disulfide, ranging from 1.80 nm (epitaxial alignment of gold) to 1.53 nm (twisted epitaxial alignment of gold). Additionally, bright field STEM imaging reveals a faint, larger "moiré of moiré" structure in cases where the bilayer molybdenum disulfide twist angle is small (~6°), arising from the overlapping three-layers, which is not visible in conventional transmission electron microscopy images. Our experiments indicate that scanning transmission electron microscopy as a suitable tool for moiré analysis of twisted multilayer planar heterostructures, complementary to information provided by conventional transmission electron microscopy and diffraction.

1. Introduction:

Two dimensional materials such as graphene and molybdenum disulfide (MoS_2) show promise for future nano-scale applications not only for their intrinsic properties but also how they may be manipulated to create novel artificial systems (Geim, et al. 2013). One way the latter has been achieved is by physically twisting the 2D-atomic layers with respect to each other to create twisted bilayers or multilayers (Carr, et al. 2017). Previously unexpected properties have resulted such as superconductivity in a "magic-angle" twisted bilayer graphene (1.1^o twist) (Cao, et al. 2018) and a fractional quantum anomalous Hall effect in twisted bilayer molybdenum ditelluride (3.7^o twist) (Park, et al. 2023). Such structures are sometimes known as "moiré materials" owing to the additional periodic atomic matching at their interfaces (Andrei, et al. 2021).

Since accessing any specific property (especially electronic) would often require a metal or conductive contact, the reaction and structure of metals with 2D materials is clearly important. By conventional transmission electron microscopy (TEM) and selected area electron diffraction (SAED), we recently found that upon annealing gold (Au) nanoparticles between twisted MoS_2 bilayers, the original epitaxial orientation relationship with the first MoS_2 layer was transformed into a twisted epitaxial arrangement, with the realignment typically halfway between the orientations of the two component MoS_2 layers, up to a twist angle of 7^o or so. There is then a milder, sinusoidal variation of Au realignment up to 60^o twist (Cui, et al. 2023; Cui, et al. 2024). This is consistent with a reduction of the total interfacial energies according to our density functional theory (DFT) calculations.

As these structures are relatively amenable to study by high resolution, scanning transmission electron microscopy (STEM), we have applied this technique to study them in more detail. While the epitaxial alignment of gold on MoS_2 and moiré patterns in 2D materials have been previously studied (e.g. Liu et al, 2014, Chou et al. 2015, Chen et al 2020, Reidy et al. 2021, Weston et al. 2022 Kinoshita et al. 2024), a high-resolution STEM analysis of the twisted epitaxial MoS_2-Au-MoS_2 heterostructure, along with the detailed characterization of its complex moiré pattern, has yet to be explored. This work addresses this situation, as discussed in the following sections. Besides the classical moiré patterns and through-foil selected area diffraction information, we have also analyzed the Au plasmon energies by electron energy loss spectroscopy (EELS) in order to establish whether any new electronically excited states might be revealed in the new

epitaxial structures. The application of high-resolution STEM analyses such as these can contribute to understanding the material structure and to indicate by EELS whether or not any noticable properties might arise from them.

Experimental procedure

The experimental approach largely follows the procedures described by Cui et al. (2024), with additional information pertinent to this paper given here. Thin MoS_2 flakes (~3 nm in thickness or so) were prepared by standard exfoliation onto a thin amorphous silicon nitride TEM grid. Gold was electron-beam deposited onto the first MoS_2 substrate under non-UHV vacuum conditions resulting in approximately equiaxed Au nanoparticles (~ 3.5 nm in diameter) epitaixal with the hexagonal MoS_2 layer as determined by a combination of BF-TEM and atomic force microscopy (AFM). The second layer was then attached by exfoliation with a large range of crystallographic twist angles from 0º to 60º. Annealing treatments in an argon atmosphere at 500 ºC resulted in the most dramatic changes in gold re-orientation and morphology. A schematic example of the structures of Au in the MoS_2 bilayer chosen for further study here is shown in the schematic diagram (Figure 1).

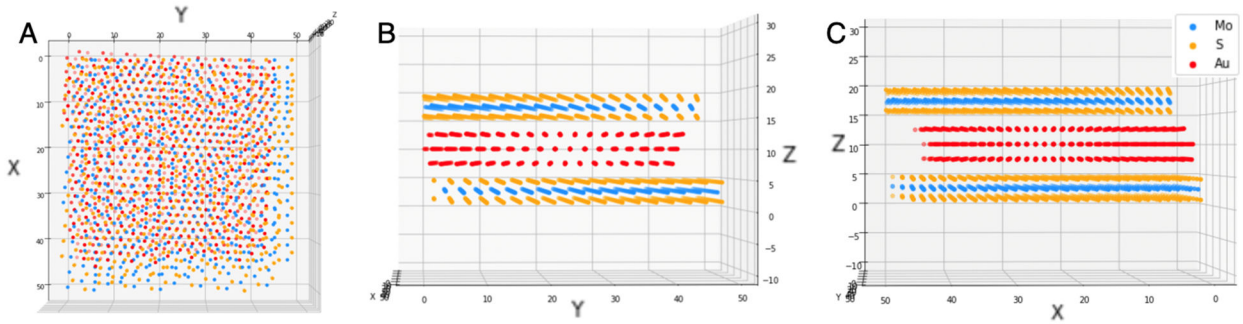

Figure 1 | Projected atomic model of twisted epitaxial MoS_2-Au-MoS_2 heterostructures with a bilayer MoS_2 twist angle of 6º and an orientation mismatch of Au with each layer of 3º. A. Plan-view in the X-Y planes showing the moiré structure. The X direction aligns with Au [1-10] and Y direction aligns with Au [11-2]. B. Side-view from the Y-Z plane of three close packed {111} planes if FCC Au between a top and bottom layer of MoS_2. C. Side-view from the X-Z plane. The scale of each horizontal axis is in Angstrom units (0.1 nm). The Mo atoms, S atoms and Au atoms are marked in blue, orange, and red, respectively.

The original TEM imaging and diffraction observations were made on a conventional FEI Tecnai microscope operated at 200 kV. In the present paper, the STEM analyses were carried out on a Thermo Fisher double-corrected, monochromated Spectra TEM-STEM operating at 300 kV. Each

high angle annular dark field-STEM (HAADF-STEM) and bright field-STEM (BF-STEM) image comprised 2048 by 2048 pixels, acquired using a probe current of ~100 pA with a pixel dwell time of 10 μs. The spatial resolution is determined largely by the probe size, and is measured to be 80 pm from the fast Fourier transform (FFT) of the high-resolution STEM image. Standard imaging conditions in terms of electron beam dose rates etc. could be employed as the materials are largely stable under the electron beam during the present data acquisition procedures. Monochromated STEM-EELS measurements were conducted at 60 kV, with a probe current of 40 pm, a convergence angle of 24 mrads, and a camera length of 28 mm, at an energy resolution of about 60 meV. The pixel size was set to be 1 nm and the dwell time was 0.3 s. The field of view of EELS scan was 50 pixels by 50 pixels.

Results

Because the molybdenum disulfide flakes are made by exfoliation, the as-grown samples both have good electron transparency and are very close to the basal plane [0001] zone axis orientation. The FCC gold nanoparticles are orientated with their close packed $\{1\bar{1}1\}$ planes parallel to the MoS_2 basal plane and their {220} planes (spacing 0.144 nm) parallel to $\{11\bar{2}0\}$ MoS_2 (spacing 0.158 nm). Thus in conventional bright field images three sets of moiré fringes are seen making up a pseudo-hexagonal array, and the Au 220 reflection vectors are parallel to the 110 reciprocal lattice vectors of MoS_2 (Takayanagi, et al. 1988, Reidy, et al. 2021). The twisted epitaxy is manifested both by a reduction of the moiré spacings and by an offset of the Au 220 reflections from the 110 MoS_2 reciprocal lattice vectors, as seen in the diffraction patterns (e.g. Figure 2).

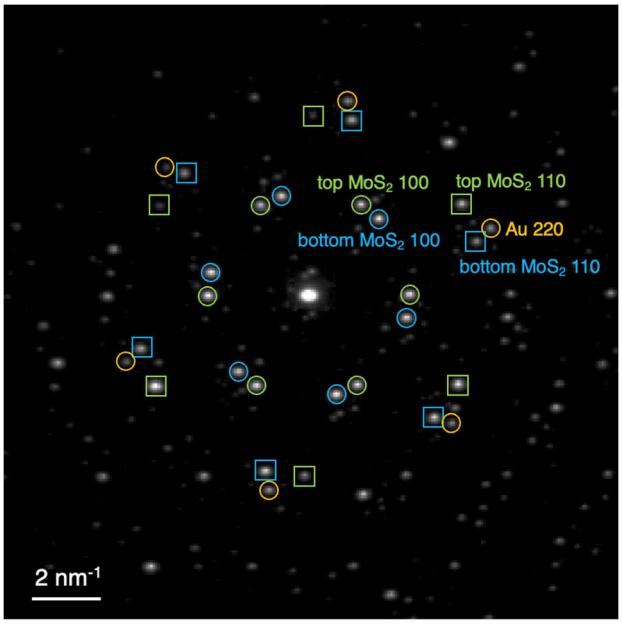

Figure 2 | Selected area electron diffraction (SAED) pattern showing the twisted epitaxial relationship of Au with twisted bilayer MoS_2. The bilayer twist angle is 12.5° and the orientation of Au {220} with bottom MoS_2 {110} is 2.2°. The diameter of the selected area was about 200 nm. The diffraction spots from top MoS_2 {100}, top MoS_2 {110}, bottom MoS_2 {100}, bottom MoS_2 {110}, and Au {220} are marked in green circles, green squares, blue circles, blue squares, and orange circles, respectively. The twisted epitaxy is best seen from the positions of the latter two reflections.

Figure 3 shows [0001]/[111] zone axis HAADF-STEM (A) and BF-STEM (B) images of an epitaxial gold nanoparticle on a thin molybdenum disulfide layer, with a thin graphene layer exfoliated on top, after annealing at 500 ºC for 2 hours. The collection semi-angles of the HAADF and BF images are 63-150 mrads and 0-25 mrads, respectively. As the graphene is unlikely to contribute to the HAADF image, the moiré pattern within the brighter Au region is seen clearly superimposed on the HAADF MoS_2 image (Fig. 3A). The average period of the hexagonal moiré lattice is 1.80 nm which is consistent with a perfect epitaxial Au-MoS_2 alignment, with the {220} planes of Au aligned with the {110} planes of MoS_2 (Note that the moiré fringe spacing of 1.62 nm in Cui, et al. 2024 represents the perpendicular separation of consecutive rows of the bright moiré image spots rather than their hexagonal lattice periodicity). The darker MoS_2 background layer also displays the Mo and S structure of the 2D material, as shown more clearly in the inset. As the moiré patterns in conventional TEM images arise from the original atomic overlapping of the participating crystal structures, their appearance in STEM-HAADF is not unexpected, although not commonly studied. Likewise, the BF-STEM image shows brighter MoS_2 background and moiré fringes in the Au-MoS_2 region with the same spacing as that in HAADF image (Fig. 3B). Note that the bright spots in the DF moiré pattern closely overlap with the bright spots in the BF moiré as well.

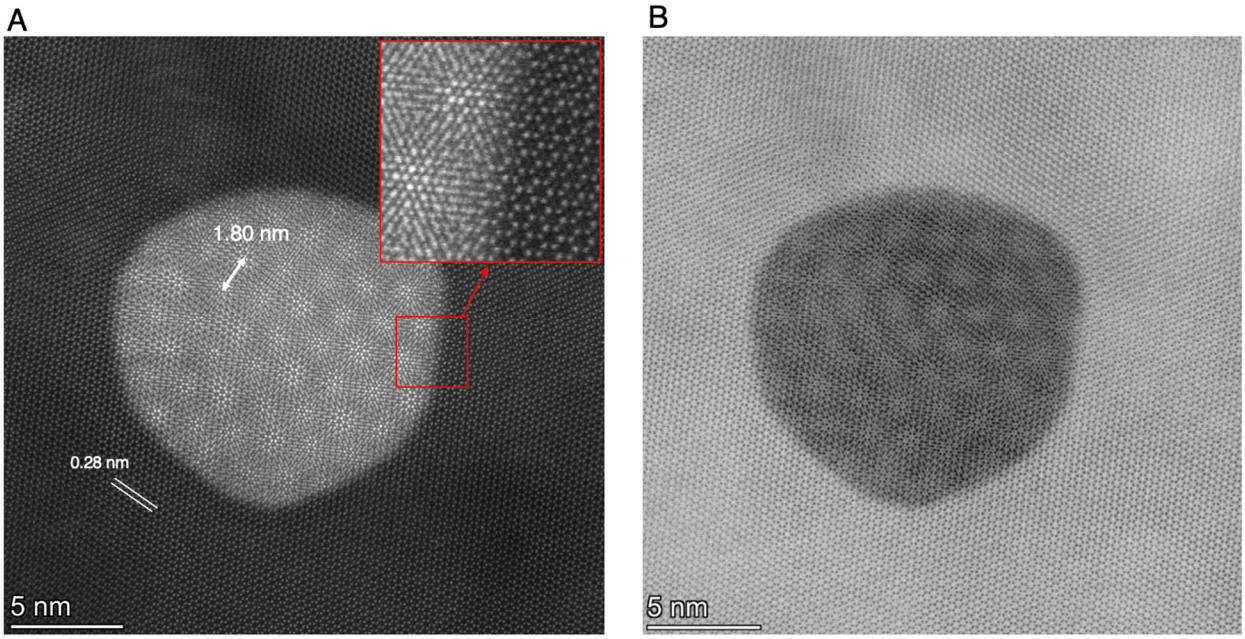

Figure 3 | A. STEM HAADF image of a small Au nanodisc encapsulated in graphene (top layer) and MoS_2 (bottom layer), appearing as a brighter region at the center of the image.

The Au nanodisc is epitaxially aligned with the MoS_2. The [100] lattice spacing of MoS_2 was measured to be 0.280 nm and the hexagonal moiré pattern from Au with MoS_2 was measured to be 1.80 nm in period, confirming the epitaxial alignment. The inset shows an enlarged image of the edge of the Au nanodisc, showing both Au and MoS_2 lattices. Brighter regions correspond to atomic overlap. B. STEM BF image of the same region showing the Au nanodisc as a darker region in the image and the bright moiré spots similarly positioned. The atomic structure of the MoS_2 is clearly shown in both HAADF and BF STEM images.

Epitaxial alignment of Au with the bottom MoS_2 is also observed in the sample where the top graphene is replaced by a MoS_2 flake with a ~30° orientation mismatch with the bottom MoS_2. The bilayer twist shows close to 0° twisted epitaxy upon annealing owing to the system crystallography and sinusoidal-like relation of the Au re-alignment with the MoS_2 layer twist angle. Figure 4A shows the HAADF-STEM images of a typical Au nanodisc in this sample. Higher magnification HAADF images of the center and edge region in the nanodisc are shown in Figs. 4B and 4C, respectively, showing the lattice of MoS_2 and the moiré pattern from the Au with bottom MoS_2. The lattice of the top MoS_2 is not observable in the image, which likely is because it is thinner than the bottom MoS_2 flake in this sample. The moiré pattern from the bilayer MoS_2 is not observable as well, owing to the large twist angle. The moiré pattern in the Au-MoS_2 shows a period of 1.80 nm, confirming the epitaxial alignment. It is worth noting that the moiré fringes have a small 2.5° misorientation with the MoS_2 110 lattice planes, indicating a 0.22° misalignment of Au {220} planes with the {110} planes of the bottom MoS_2 (Fig. 4B). A previous study suggests that a lattice misorientation of up to 0.3° is considered reasonable in the epitaxial Au-MoS_2 system (Reidy, et al. 2021), and seems to demonstrate that the moiré patterns are very sensitive both to spacing and orientation.

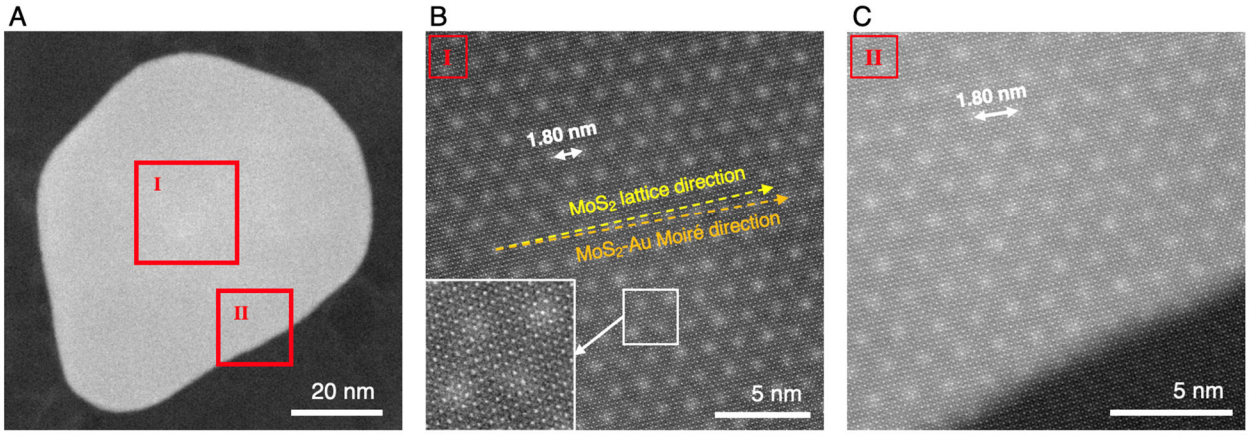

Figure 4 | A. HAADF image of a Au nanodisc encapsulated in bilayer MoS_2. The twist angle of the bilayer is 30º, and the Au nanodisc is epitaxially aligned with the bottom MoS_2. B. Higher magnification HAADF image of region I in A, showing the lattice of MoS_2, and the hexagonal moiré pattern of Au with the bottom MoS_2 with a period of 1.80 nm. The inset shows an enlarged image of the region marked in the white box, showing the lattice and moiré patterns more clearly. C. HAADF image of region II in A, showing the edge of the Au nanodisc with a relatively uniform moiré period of 1.8 nm.

The decrease in moiré period due to the twisted epitaxial re-orientation after annealing the Au nanoparticles between two twisted MoS_2 thin layers is illustrated in Fig. 5. The average period of the hexagonal moiré pattern in the HAADF and BF-STEM images is 1.53 nm, consistent with a twist of 3º of the gold lattice with respect to the upper and lower MoS_2 layers, which are mutually twisted by 6º here, as confirmed by the SAED pattern. In fact, the moiré fringe periods and twist angles measured from selected area diffraction patterns are exactly those predicted by the simple formula $S = \Delta g^{-1}$ as shown by the data for several twist angles in fig. S9 of Cui et al, 2024.

In the BF image (Fig. 5B) the moiré pattern for the twisted MoS_2 layers (2.84 nm in period) is also seen outside the Au nanodisc. Within the sandwiched region, two Au-MoS_2 interfaces exist, one between Au and the top MoS_2 layer, and the other between Au and the bottom MoS_2 layer, with identical twist angles. However, owing to the projected averaged information along the beam direction in the BF image, only one moiré pattern is observable. Moreover, a moiré pattern arises from the overlapping of the two interface moirés can also be observed faintly in the BF image, which is known as "moiré of moiré" (Zhu, et al. 2020). The period of such moiré of moiré is measured to be 13 nm (Fig. 5C).

Note that the "moiré of moiré" here is different from the typical appearance in twisted trilayer 2D materials like twisted trylayer graphene (Zhu, et al. 2020), where moiré patterns usually arise from the {100} planes of each lattice. Instead, in the present case, the moiré of moiré comes from the overlap of the moiré pattern from {220} planes of Au with {110} planes of top and bottom MoS_2, respectively, as illustrated in Fig. 5D. The red arrows note the moiré vectors that connect Au 220 spots with bottom MoS_2 110 spots, while the purple arrows note the moiré vectors that connect Au 220 spots with top MoS_2 110 spots. These two vectors have slightly different orientation and length, as marked in blue ovals in Figure 5D, which can be connected by a much smaller vector, which gives rise to the larger spacing of the "moiré of moiré". It is also consistent with the $S = \Delta g^{-1}$ expression.

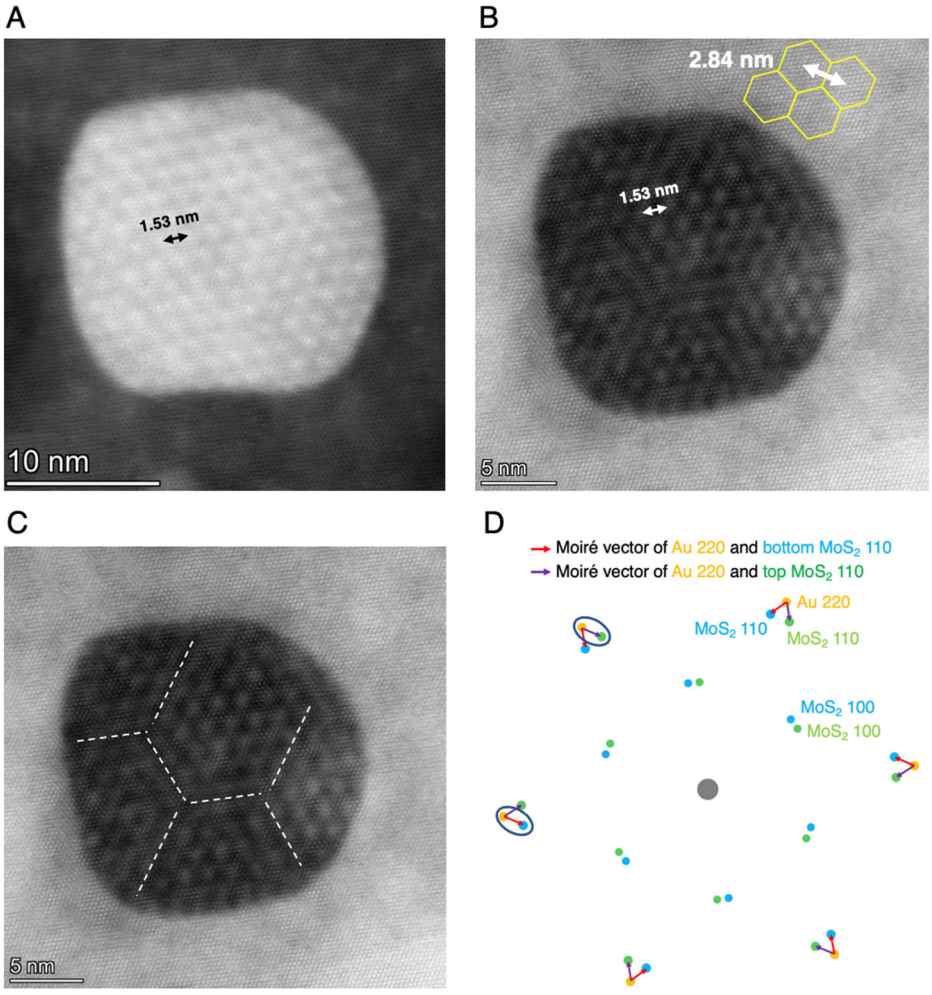

Figure 5 | A. HAADF image of Au nanodisc encapsulated in bilayer MoS_2 with a bilayer twist angle of 6°. The twist angle of Au with both MoS_2 layers is 3°, showing the twisted epitaxial

alignment. The hexagonal moiré period is measured to be 1.53 nm, confirming the twist of the Au nanodisc. B. BF image of the same region in A, showing the moiré period of the bilayer MoS_2 to be 2.84 nm. In addition, a larger moiré pattern is discernable with a period of ~13 nm, which is attributed be the moiré of two interface moirés of Au with the top and bottom MoS_2. C. The same image of B, with the moiré of moiré pattern highlighted by white dashed lines. D. Schematic diffraction pattern showing the top, bottom, and Au diffraction spots (110/220) in green, blue and orange, respectively. The moiré vectors of Au with the top and bottom MoS_2 are marked by purple and red arrows, respectively. These two vectors have similar but slightly different length and orientation, as highlighted in blue ovals, giving rise to the formation of the "moiré of moiré".

An asymmetrical misalignment of Au with the twisted bilayer MoS_2 is observed when the bilayer twist angle is larger than 7º but smaller than 30º. An example is shown in Fig. 6, where the bilayer twist angle is 12º, and the misorientation of Au with the bottom MoS_2 is 2º, as shown by SAED and schematically illustrated here in Fig. 6C. Fig. 6A shows the HAADF image of a Au nanodisc in this case, and the magnified HAADF image of the region marked in the red box is shown in Fig. 6B, where the moiré period of bilayer MoS_2 outside Au nanodisc is measured to be 1.62 nm. The period of the moiré pattern from hexagonal Au-MoS_2 should be 1.65 nm but it is not visible possibly due to the interference from the moiré pattern of the twisted bilayer MoS_2. As the MoS_2 layers are thicker in this sample, the moiré pattern from the bilayer dominates. The two primary moiré vectors have similar lengths, but very different orientations, so the length of the "moiré of moiré" vector is comparable to the primary moiré vectors, leading to a small period of the "moiré of moiré" which is hard to discern in the image (Fig. 6C).

It is worth noting that unlike the epitaxial Au nanodiscs shown in Fig. 3 and Fig. 4, which display somewhat more crystallographic perimeters, the twisted epitaxial Au nanodiscs usually display less regular shapes and curved edges, as shown in Fig. 5 and Fig. 6. In general, the moiré patterns do not show "perfect" crystal translations or periodicity, as is commonly the case (e.g. Hirsch et al. 1965). Also, very few defects in the patterns are found, showing that the Au-MoS_2 interfaces have few crystalline imperfections.

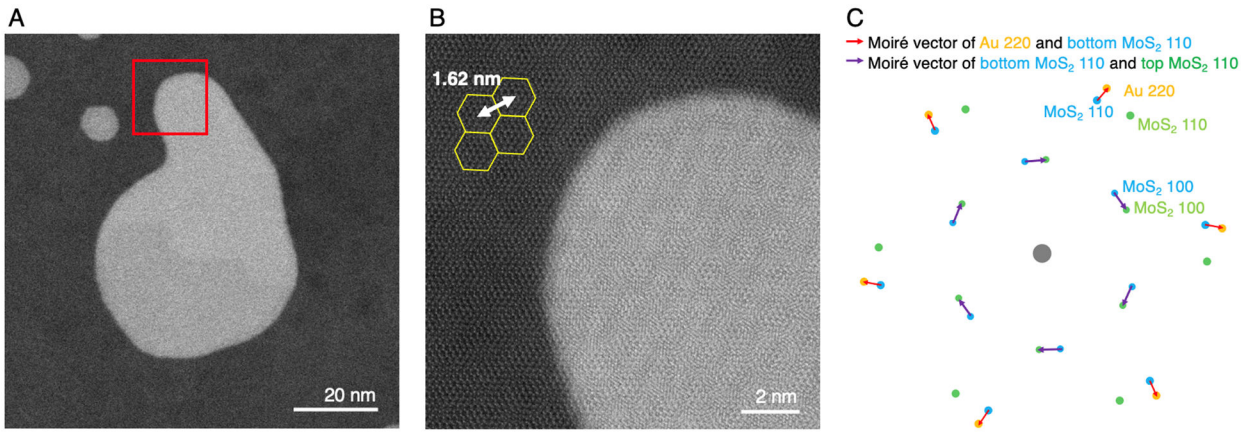

Figure 6 | A. HAADF image of a Au nanodisc encapsulated in bilayer MoS_2 with a bilayer twist angle of 12º. The twist angle of Au with bottom MoS_2 layer is determined to be 2º from selected area electron diffraction, showing a twisted epitaxial alignment. B. Higher magnification HAADF image of the region marked in the red box in A, showing the hexagonal moiré period of the bilayer measured to be 1.62 nm. C. Schematic diffraction pattern showing the top, bottom, and Au spots in green, blue and orange, respectively. The moiré vectors of Au with the bottom MoS_2 are marked by red arrows. The moiré vectors of the bilayer are marked in purple. These two vectors have similar length but different orientation, thus a smaller moiré of moiré period which might be present is not readily visible.

In order to begin exploration of any unexpected electronic effects of the gold nanodisc encapsulated in bilayer MoS_2, we carried out STEM-EELS at varying locations on the gold nanodiscs. Typical results are shown in Fig. 7. The sample used here has a bilayer twist angle of 1º and the Au is aligned halfway in between. STEM-EELS analysis at the nanodisc perimeter (Fig. 7A) shows a plasmon peak close to 1.0 eV, whereas that at the disc center is about 1.5 eV (Fig. 7B). The plasmon mappings at 1.0 eV and 1.5 eV are shown in Fig. 7C and 7D, respectively, confirming the presence of 1.0 eV peak from the edge of the disc and 1.5 eV peak from the center. (The MoS_2 exciton peaks are at 2 eV and are not of primary interest here.) The former is known to be the dipolar plasmon peak which is optically active (e.g. Zeng et al, 2020), while the higher energy bulk "breathing mode" is optically inactive. Both these values have noticeably lower plasmon energies than those of other gold nanodiscs, but they have both larger diameter (about 50 nm in Fig. 6) and are sandwiched between higher refractive index MoS_2 substrates (refractive index = 4.77). For instance, gold nanodiscs electron beam deposited onto a silicon nitride

(refractive index ~ 2.0) substrate show a dipolar plasmon peak energy decreasing from 2.1 eV to 1.6 eV as the disc diameter increases from 50 to 200 nm (Zeng at al, 2020). Similar discs on a silicon substrate (refractive index ~ 4.0) have even lower energies (from 1.8 eV to 1.4 eV as the disc diameter increases from 50 nm to 150 nm, Sinclair et al, 2021), although it is not clear how much this trend of decreasing plasmon energy with disc diameter continues above 200 nm. These sub-optical plasmon peaks are likely to be those expected from both the large size of the Au nanodiscs and the high refractive index of the medium (MoS_2) in which they exist. Moreover, the 1° twist angle of bilayer MoS_2 represents only a modest rotation, and no significant change in the plasmon energy of Au compared to that of 0° epitaxial alignment would be expected. Future research will focus on investigating whether varying the bilayer twist angle impacts the optical properties of Au, which is more sensitive than the EELS peak measurements at the current energy resolution.

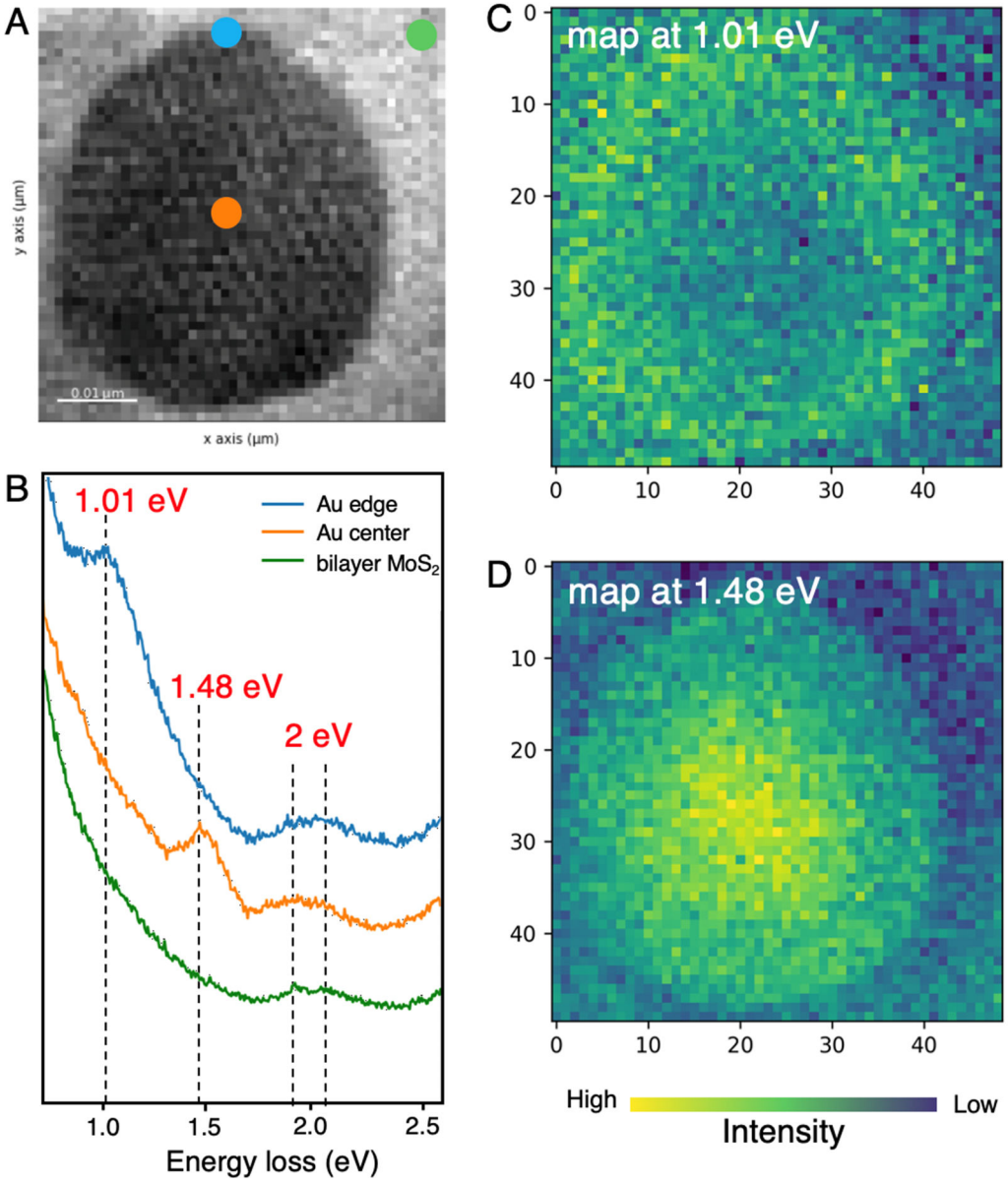

Figure 7 | A. STEM-EELS map of an Au nanodisc (~ 40 nm in diameter) at 0 eV (zero loss peak), showing the nanodisc as dark region and the background MoS_2 as bright region. The moiré fringes arising from Au and MoS_2 are also visible in this image. B. EEL spectra of the center region of Au, the edge region of Au, and MoS_2 region in (A), as marked in orange, blue, and green respectively. C. EELS map at 1.01 eV, showing the surface bipolar plasmon at the edge of Au. D. EELS map at 1.48 eV, showing the breathing mode plasmon at the center of Au. The energy window for mapping in A, C, D is 0.16 eV.

Summary

In this work, we present atomic resolution STEM imaging on twisted epitaxial Au nanodiscs grown between twisted bilayer MoS_2 with varying bilayer twist angles. With a double-corrected STEM, the moiré patterns from twisted bilayer MoS_2 and those from twisted Au-MoS_2 interface can be clearly resolved using HAADF-STEM as well as the projected atomic structures of the various layers. Additionally, BF-STEM enables the imaging of the "moiré of moiré" pattern resulting from this trilayer material at certain twist angles. Furthermore, monochromated STEM-EELS with an energy resolution of 60 mV resolves the dipolar plasmon peak of Au nanodiscs down to 1.0 eV. These results highlight that STEM can be used as a suitable tool for moiré analysis and structure-property relationship investigation of such intricate moiré materials and when combined with 4D-STEM can be complementary to conventional TEM imaging and selected area diffraction analysis.

Acknowledgements:

The authors acknowledge support from the US Department of Energy, Office of Basic Energy Sciences, Division of Materials Science and Engineering under contract DE-AC02-76SF00515. P.C. appreciates the receipt of a Fullbright Fellowship for the period in which this work was carried out.

References:

Andrei, E.Y., Efetov, D.K., Jarillo-Herrero, P., MacDonald, A.H., Mak, K.F., Senthil, T., Tutuc, E., Yazdani, A. and Young, A.F. The marvels of moiré materials. Nature Reviews Materials, 6, 201-206 (2021).

Cao, Y., Fatemi, V., Fang, S., Watanabe, K., Taniguchi, T., Kaxiras, E., Jarillo-Herrero, P. Unconventional superconductivity in magic-angle graphene superlattices. Nature 556, 43-50 (2018).

Carr, S., Massatt, D., Fang, S., Cazeaux, P., Luskin, M., & Kaxiras, E. Twistronics: Manipulating the electronic properties of two-dimensional layered structures through their twist angle. Physical Review B 95, 075420 (2017).

Chen, P., Liang, Y., Yang, B., Jia, F., Song, S. In situ reduction of Au (I) for efficient recovery of gold from thiosulfate solution by the 3D MoS_2/chitosan aerogel. ACS SCE. **8**, 3673-3680 (2020).

Chou, S., Sai, N., Lu, P., Coker, E., Liu, S., Artyushkova, K., Luk, T., Kaehr, B., Brinker., C. J. Understanding catalysis in a multiphasic two-dimensional transition metal dichalcogenide. Nat. Commun., **6**, 8311 (2015).

Cui, Y., Sinclair, R., Cui, Y. Twisted Epitaxial Growth of Gold Nanodiscs Confined in Twisted Bilayer Molybdenum Disulfide. Microsc. Microanal. 29 (Suppl 1), 1657-1658 (2023).

Cui, Y., Wang, J., Li, Y., Wu, Y., Been, E., Zhang, Z., Zhou, J., Zhang, W., Hwang, H.Y., Sinclair, R., Cui, Y. Twisted epitaxy of gold nanodisks grown between twisted substrate layers of molybdenum disulfide. Science, 383, 212-219 (2024).

Geim, A., Grigorieva, I. Van der Waals heterostructures. Nature 499, 419–425 (2013).

Hirsch, P.B., Howie, A., Nicholson, R. B., Pashley, D. W., Whelan, M. J. Electron Microscopy of Thin Crystals. Butterworth/Heinemann; First Edition (1965)

Kinoshita, K., Lin, Y. C., Moriya, R., Okazaki, S., Onodera, M., Zhang, Y., Senga, R., Watanabe, K., Taniguchi, T., Sasagawa, T., Suenaga, K. Crossover between rigid and reconstructed moiré lattice in h-BN-encapsulated twisted bilayer WSe_2 with different twist angles. Nanoscale, **16**, 14358-14365 (2024).

Liu, K., Zhang, L., Cao, T., Jin, C., Qiu, D., Zhou, Q., Zettl, A., Yang, P., Louie, S. G., Wang, F. Evolution of interlayer coupling in twisted molybdenum disulfide bilayers. Nat Commun. **5**, 4966 (2014).

Park, H., Cai, J., Anderson, E., Zhang, Y., Zhu, J., Liu, X., Wang, C., Holtzmann, W., Hu, C., Liu, Z.,Taniguchi, T. Watanabe, K., Chu, J.-H., Cao, T., Fu, L., Yao, W., Chang, C.-Z., Cobden, D., Xiao, D., Xu, X. Observation of fractionally quantized anomalous Hall effect. Nature 622, 74–79 (2023).

Reidy, K., Varnavides, G., Thomsen, J.D., Kumar, A., Pham, T., Blackburn, A.M., Anikeeva, P., Narang, P., LeBeau, J.M. Ross, F.M. Direct imaging and electronic structure modulation of moiré superlattices at the 2D/3D interface. Nat. Commun., 12, 1290 (2021).

Sinclair, R., Zeng, Y., Madsen, S. J., Gambhir, S. S. An approach for optimizing gold nanoparticles for possible medical applications, using correlative electron energy loss and Raman spectroscopies on electron beam lithographically fabricated arrays. J. Mater. Res. 36, 3383-3397 (2021).

Takayanagi, K., Tanishiro, Y., Yagi, K., Kobauashi, K., Honjo, G. UHV-TEM study on the reconstructed surface of Au (111): Metastable p″ × p″ and stable p × 1 surface structure. Surf. Sci. 205, 637-651 (1988).

Weston, A., Castanon, E.G., Enaldiev, V., Ferreira, F., Bhattacharjee, S., Xu, S., Corte-León, H., Wu, Z., Clark, N., Summerfield, A., Hashimoto, T. Interfacial ferroelectricity in marginally twisted 2D semiconductors. Nat. Nanotechnol. **17**, 390-395 (2022).

Zeng, Y., Madsen, S. J., Yankovich, A. B., Olsson, E., Sinclair, R. Comparative electron and photon excitation of localized surface plasmon resonance in lithographic arrays for enhanced Raman scattering. Nanoscale 12, 23768-23779 (2020).

Zhu, Z., Carr, S., Massatt, D., Luskin, M., Kaxiras, E. Twisted trilayer graphene: A precisely tunable platform for correlated electrons. Physical Review Letters, 125, 116404 (2020).